

Growth of Carbon, Boron Nitride and ZnO Nanotubes for Biosensors

Jason P. Moscatello, Jiesheng Wang, Benjamin Ulmen, Vijaya K. Kayastha, Ming Xie, Samuel L. Mensah, Shun Wu, Archana Pandey, Chee Huei Lee, Abhishek Prasad, Yoke Khin Yap*

Department of Physics, Michigan Technological University, Houghton, Michigan 49931, USA

*Corresponding author: ykyap@mtu.edu

Nanotubes have significant portions of their atoms located at the surfaces and represent the future of biological devices. With such small dimensions, sensitivities and applications previously impossible are being made real. Not all nanomaterials are currently at the same level of proficiency, however. Carbon nanotubes are a mature, easily grown and controlled nanostructure, but boron nitride and zinc oxide are still coming into their own. Yet progress in all three species of nanotubes is making applications easier than before.

Introduction

Nanotubular structures are highly interdisciplinary in their use. Here we review the properties and applications of three particularly noteworthy nanotubes for biological applications: carbon, boron nitride and zinc oxide nanotubes. The ability to effectively create and test applications depends ultimately on the ease and control of synthesis; therefore the current state of growth for each of these nanotubes developed in our group will be discussed, focusing on ease and control of growth parameters such as size, diameter, number of walls, etc.

Carbon Nanotubes

Since the discovery of their structural properties (1), carbon nanotubes (CNTs) have attracted great attention due to their high aspect ratio, superior mechanical and electronic properties and high chemical stability, while additional properties make them suitable particularly for biological application. For example, the ability to elastically buckle can protect delicate samples during probing (2), single-walled carbon nanotubes (SWCNTs) have been shown to be able to move into living cells (3) and every atom is on their surface (4). Together, these characteristics make CNTs versatile components for biological applications, as the following review will show.

Wong et al. used an oxidizing process to open the tips of multi-walled carbon nanotubes (MWCNTs) for use as a functionalized probe. The oxidation also formed carboxyl groups at the open ends which were then coupled to amide groups via carbodiimide chemistry to form selective bonds. The now-functionalized MWCNT was used as a probe in tapping mode atomic force microscope (AFM) experiments on a patterned self-assembled monolayer (SAM) substrate. The AFM phase image clearly show differences in phase between the two distinct SAM regions due to varying adhesion forces between each substrate SAM and the functionalized MWCNT AFM probe tip (2).

Covalent modification of CNTs, as above, may be desirable for many applications, but it is important to have noncovalent techniques available as well. In particular, the structural and electronic properties of CNTs can be disrupted by covalent bonding on their surface. Chen et al. achieved non-covalent bonding of the bifunctional molecule 1-pyrenebutanoic acid, succinimidyl ester SCME to a SWCNT in both dimethylformamide and methanol solutions. SCME is adsorbed due to strong π stacking interactions between the highly aromatic pyrene group and the graphitic SWCNT surface. Further, after functionalization, proteins could be immobilized on the SWCNT by immersion in an aqueous solution of protein, all the while preserving the graphitic carbon network of the SWCNT (4).

Nguyen et al. used arrays of the vertically-aligned (VA) CNTs to construct nanoelectrode platforms for biosensor development. Oxidation was used to attach carboxyl groups to the opened tube tips. However, in order to preserve the vertical alignment and properties of the VA-CNTs during this process, a spin-on glass (SOG) was used to fill in the gaps between the individual tubes after growth. The SOG film doubled as a dielectric, insulating the tubes from their neighbors. After oxidation, nucleic acid was attached using standard water soluble coupling reactions (5).

One approach to biosensing is to use SWCNT transistor schemes. Besteman et al. constructed field effect transistors (FETs) by CVD grown semiconducting SWCNTs on doped Si wafers with an oxide layer. Experiments were done in aqueous solution, using the liquid as the gate. Glucose oxidase (GOx) enzymes were immobilized on the SWCNT surface by use of a linking molecule. Measurements showed that attachment of only 50 molecules of GOx significantly decreased the conductance of semiconducting SWCNT, showing the schemes' potential as a GOx protein sensor. Further, the GOx-immobilized tubes show a strong dependence on the pH of the solution, making them perfect nanoscale pH sensors (6).

CNTs can also be applied *in vivo* for various applications. For example, transport into cells is possible using SWCNTs, which have been shown to shuttle cargo through cellular membranes without cytotoxicity. Wong et al. found that Cy3-DNA functionalized SWCNTs uptake into cells takes place under an endocytosis mechanism (3). Cells are invisible to near infrared (NIR), but the SWCNTs have high absorbance. Pulsing NIR at cells with the SWCNTs inside them can cause cell death. In addition, shorter pulses can trigger endosomal rupture and releasing of noncovalent cargo carried by the SWCNTs. Wong went on to show that the SWCNTs can be specifically functionalized to target chemically marked tumor cells, allowing destruction of only cancerous cells through NIR pulses (3,7).

Also a potentially *in vivo* application, Wang et al. made microelectrode arrays for use stimulating neurons. In short summary, quartz substrates were prepatterned with microcircuitry before synthesizing MWCNTs directly on the device, resulting in an array of electrically conductive MWCNT pillars, each individually addressable. The size, geometry and location of the VA-MWCNT pillars are controlled by lithographic patterning of the catalyst, and the protruding pillar is advantageous for use in layered tissues (8). Cyclic voltammetry scans in aqueous phosphate-buffered saline solution showed current flow is carried by a capacitive charge injection mechanism. This is ideal

because no chemical changes occur to either tissue or electrode during current flow. *In vitro* stimulation of embryonic rat hippocampal neurons plated atop the VA-MWCNT electrodes showed that the cells responded consistently to stimulated pulses (8).

In vivo uses would be pointless if the CNTs were toxic. *In vivo* studies of the toxicity of functionalized CNTs (fCNTs) performed by Singh et al. demonstrate that water soluble fCNTs are significantly less toxic than the non-functionalized tubes. CNTs functionalized with diethyltriaminepentaacetic and complexed with ^{111}In were injected into mice and the amounts in the body over time monitored. fCNTs were found to be rapidly cleared from all affected tissues through the renal excretion route with a half-life of 3 to 3 1/2 hours. This is not as fast a clearance as other gene therapy vectors, but is a significant improvement over non-functionalized CNTs (9).

Carbon Nanotube Growth

As discussed, various types of CNTs are required depending on the configuration of the biological applications. Thermal chemical vapor deposition (CVD) is a convenient technique for growing all types of CNTs directly on the substrate. The Vapor-Liquid-Solid (VLS) growth mechanism (10) is well accepted for this growth which simply involves decomposition of a carbon precursor on catalyst surfaces, diffusion of released carbon atoms into them, their saturation and then segregation in the form of nanotubes. However, it does not provide sufficient details on the precursor decomposition on the catalyst nano-particles which is of critical importance for maintaining catalyst activity for continuous growth. We proposed a growth model (11) which is a combination of dissociative adsorption of acetylene precursor (12) and the VLS mechanism (10). According to our growth model, equilibrium between decomposition of acetylene molecules and diffusion of released carbon atoms to the growth sites is the crucial condition towards optimized growth. Based upon our growth model, we were able to optimize growth parameters (13), enabling growth of highly dense, vertically aligned single-, double- and multi- walled CNTs.

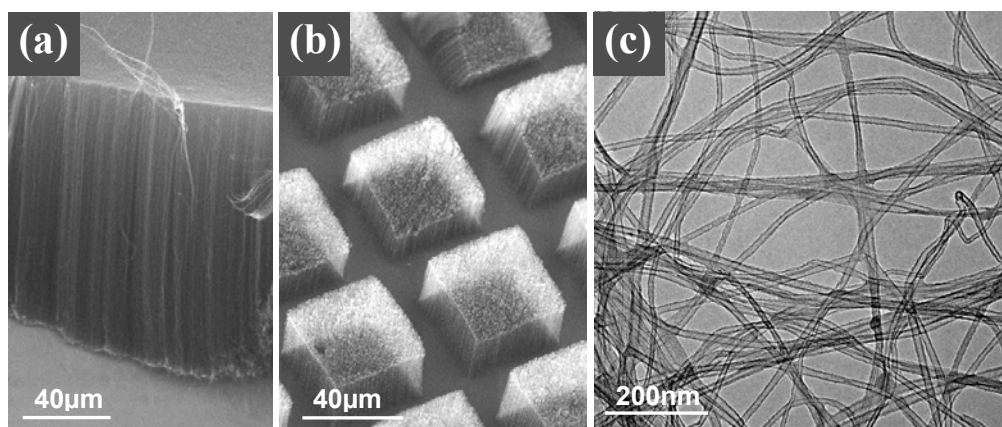


Figure 1. MWCNTs grown at 700°C by thermal CVD of acetylene. (a) A dense forest of MWCNTs, (b) micro-towers of MWCNTs and (c) Images of MWCNTs under transmission electron microscope (TEM).

MWCNTs were grown on the SiO₂/ Si substrates, using pulsed laser deposited Fe films (11). The catalyst coated substrate was annealed to transform the Fe film into Fe nanoparticles that act as the nucleation sites for nanotube growth. Growth was carried out using acetylene and some buffer gases such as Ar, H₂ or N₂. As shown in Figure 1, MWCNTs can be grown at high-density with desired patterned. These MWCNTs have high-order tubular structures as shown in Figure 1(c).

Growth of SWCNTs and DWCNTs is much more difficult than that of MWCNTs. They require very small catalyst particle size, in the range 1-3 nm, high formation energy to overcome the strain of the small diameter and limited supply of carbon atoms. To fulfill these requirements, they are usually grown at higher temperatures using stable carbon precursors such as methane, carbon monoxide, etc. Here by the use of optimized Al/Fe/Mo tri-layer catalysts and controlled acetylene supply, we have been able to grow ultra high dense, vertically aligned SWCNTs and DWCNTs at temperatures as low as 700°C. For example, by using an Al (10nm) /Fe (0.5nm) /Mo (0.1 nm) tri-layer catalyst, a high-density of SWCNTs (Figure 2) can be grown by using a gas mix of acetylene (10 sccm) and hydrogen (120 sccm). As shown, cracking of the film occurs due to the mechanical stress generated within the high-density film during the growth and cooling process. Radial breathing modes of these SWCNTs are clearly detected from Raman spectroscopy.

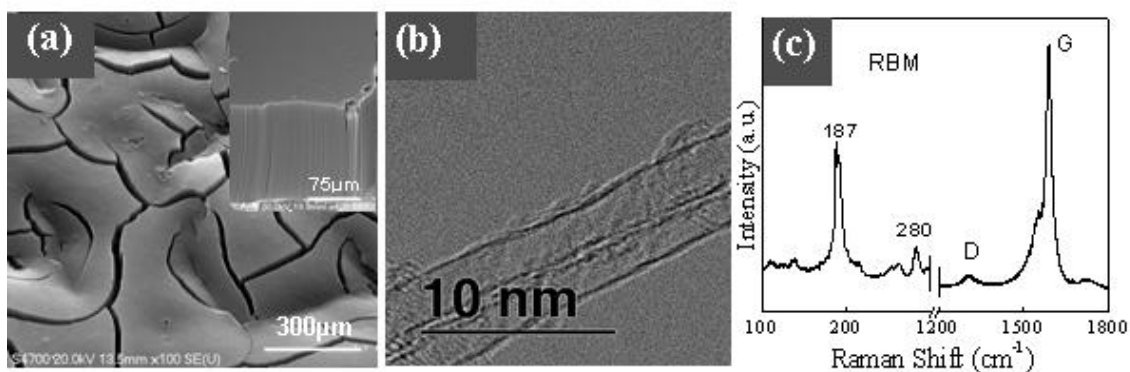


Figure 2. Acetylene- based growth of vertically aligned SWCNTs. (a) SEM images. The sample was tilted at 45° during imaging. (b) A TEM image with 2 SWCNTs and (c) Raman spectrum of SWCNT film.

As discussed earlier, arrays of VA-CNTs have been useful for biological sensing (5). In our case, we found that a dual plasma-enhanced chemical vapor deposition (PECVD) technique gives fine control over the growth of these VA-CNTs. The ability to tune several important parameters of the properties of the CNT gives this method an advantage over other methods such as thermal chemical vapor deposition or arc discharge method. Additionally CNTs grown by the PECVD method are grown directly on substrates and are aligned perpendicular to the substrate surface as shown in Figure 3 (14).

Like the name suggests, a dual plasma-enhanced chemical vapor deposition chamber has two water-cooled electrodes for two radio-frequency plasma sources. This design provides for separate control over primary gas decomposition and substrate biasing. The top electrode is the site of the primary gas decomposition. The plasma generator is

operated in RF mode by adjustment of the RF plasma power. The bottom electrode is responsible for substrate biasing. It is operated in DC mode by adjusting the bias voltage. A wire creates an electrical connection from the electrode surface to metal plate that holds the substrate on a boron-nitride ceramic heater. The heater electrical connectors are ceramic-coated and are electrically isolated from the plasma. The PECVD chamber is equipped with a mass flow controller for precision adjustment of gas flow into the system. The system is capable of controlling the flow of several different process gasses at the same time.

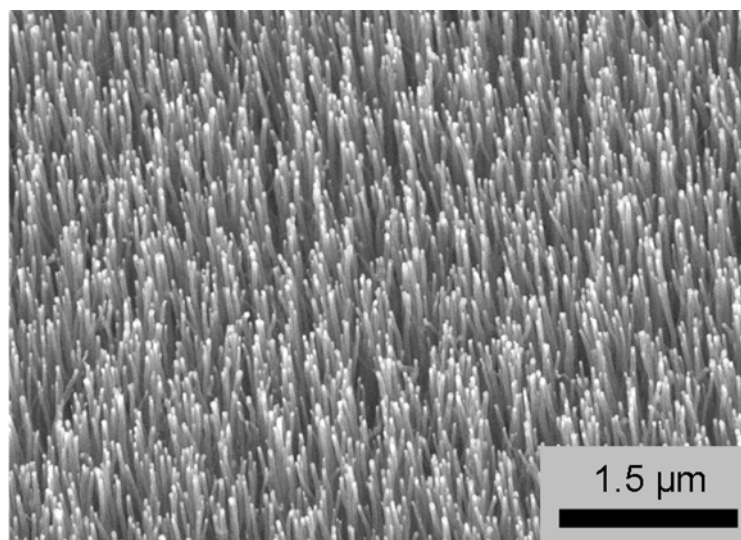


Figure 3. This is a typical scanning electron micrograph of VA-CNTs grown by the PECVD method.

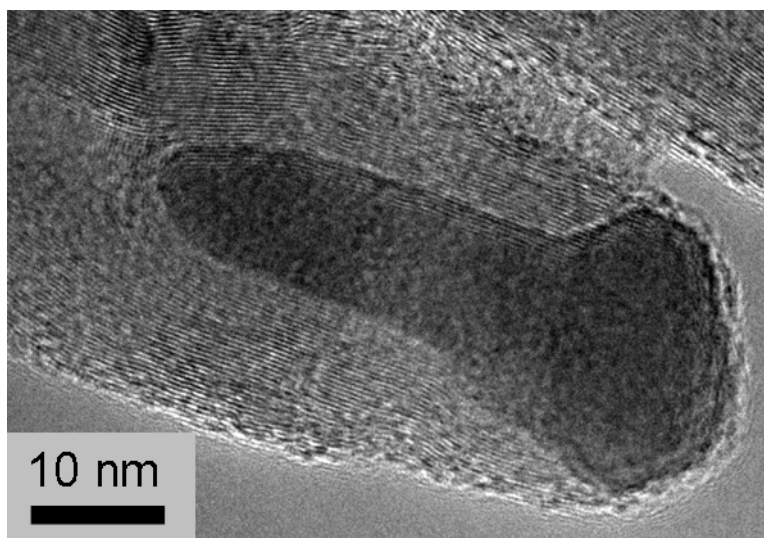


Figure 4. This TEM image shows a MWCNT grown by PECVD method. It is characterized by high graphitic order of the walls and low amorphous deposition on the walls.

Diameter is controlled by adjustment of several factors, the most important of which involves preparation of the substrates with a precisely known film thickness of metal catalyst (Ni in this case) which can be controlled down the angstrom level. The thickness of the catalyst film determines the rough size of the catalyst nanoparticles that become the growth sites of the carbon nanotubes. As shown in Figure 4, these catalyst particles always remain at the tips of the nanotubes. Diameter can also be controlled on a finer level by adjustment of *in situ* heater temperature and by control over the substrate bias voltage (15).

Control over CNT length can be achieved by duration of the growth session. Since this method has a much slower growth rate than thermal CVD process, finer control is allowed over the final CNT length. Additionally the relatively short CNTs produced by PECVD are structurally stable enough to remain vertically-aligned through the process, a property essential to many future biological applications.

In short, CNTs can be readily grown as SWCNTs, MWCNTs, arrays of micro-towers, and VA-CNTs. Therefore, CNTs can be readily used for various biological applications.

Boron Nitride Nanotubes

Boron nitride nanotubes are also chemically inert and bio-compatible for biological applications. BNNTs were first grown in 1995, and possess a similar structure to CNTs (16). What is more, they possess uniform electronic properties which are insensitive to their diameters and chiralities (17). Although they have wide band gaps (~5 eV), theoretically, their band gaps can be tuned and even eliminated by transverse electric fields via the giant dc Stark effect (18-20). In addition, BNNTs are resistant to oxidation up to 800°C (21), have excellent piezoelectricity (22, 23) and potential hydrogen storage capability (24). These properties make BNNTs well recognized as a good complement to CNTs in future nanotechnology.

Zhi et al. have done much work on modifying BNNTs for biological applications. In an attempt to make BNNTs soluble in organic liquids, the group began by functionalizing the tubes. The high temperature CVD grown BNNTs were wrapped (a non-covalent interaction) with the conjugated polymer poly[*m*-phenylenevinylene-*co*-(2,5-dioctoxy-*p*-phenylenevinylene)] (PmPV). The wrapping took place by dissolving PmPV in a solution of BNNTs in chloroform and sonicating for 2 h at room temperature. The resulting tubes were slightly shorter than the original tubes due to the sonication, but were found to be soluble in many organic solvents. The strong adhesion to the BNNT is due to π - π interactions between the polymer and BNNTs, which does not affect the band gap of the tubes (25).

Further work led to covalently functionalizing the BNNTs. The process methodology was based on chemical reactions between the COCl group of stearoyl chloride and the amino groups on the BNNTs. Comparisons of the FTIR spectra show differences between the functionalized and original BNNTs in the electronic states. In addition, CL and UV/vis absorption spectra also indicate that long alkyl chains may induce drastic changes in the band structure of BNNTs (26).

Continuing, Zhi et al. immobilized proteins on BNNTs. This was accomplished by simply by mixing dispersed BNNTs in a dilute protein solution for hours. After 120 hours, the ferritin protein was confirmed to be immobilized, with no dependence of ferritin density on tube size. To reduce the time required, 1-pyrenebutyric acid N-hydroxysuccinimide ester functionalized tubes were used, lowering the necessary mixing time to 24 hours (27).

Studying the effects of this covalent bonding of the BNNT sidewalls by computational methods, it was found that the band gap decreases as the number of concentrations become two- and six- fold. The six-fold case actually shows no discernable energy gap and thus opens the possibility of functionalized BNNTs exhibiting metallicity. In the future, smooth tuning of the BNNT band gap may be possible (28).

Boron Nitride Nanotube Growth

While BNNTs show a lot of promise and researchers have begun incorporating them into biological applications, there is still a long way to go. The single biggest obstacle is that growing BNNTs has been puzzling people for the last 10 years. BNNTs have been grown by arc discharge (29,30), laser ablation (31,32), substitution reactions from carbon nanotubes (33), ball-milling (34), and chemical vapor deposition (35), methods that require high temperatures ($>1100^{\circ}\text{C}$) and are dominated by impurities such as amorphous boron nitride powder and catalyst particles. All these techniques are not applicable for direct growing BNNTs on substrate for device fabrication. Recently, our group reported the synthesis of BNNTs directly on substrate at 600°C by a plasma-enhanced pulsed-laser deposition (PE-PLD) technique (36).

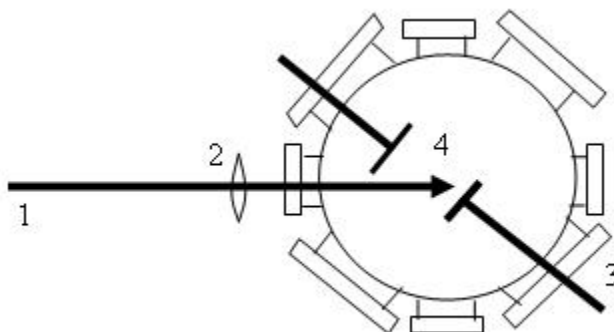


Figure 5. Schematic of the PE-PLD system. The laser beam (1) is focused by a lens (2) onto a rotating BN target (3). The BN growth species from the target will be accelerated toward the substrate (4) by applied substrate bias voltages.

The PE-PLD system consists of an ultra-high vacuum stainless steel chamber (Figure 5) and a fourth harmonic generation of a Nd:YAG laser. Pure iron (12.5 nm) films are first deposited on oxidized silicon substrates at room temperature by PLD in vacuum with thicknesses controlled by an *in situ* monitoring system. Substrates with Fe films are then installed on the heater and sealed inside the vacuum chamber at a base pressure as high as $\sim 5 \times 10^{-7}$ mbar before filling it with pure nitrogen gas to a pressure of 2×10^{-2} mbar. The

substrates are heated and maintained at 600 °C by a pyrolytic BN heater controlled by a proportional-integration-differentiation (PID) system. Plasma was generated on the substrate surface for 10 minutes by an RF generator (13.56 MHz) that is capacitively coupled to the steel substrate holder, inducing a negative dc voltage on the substrates. Fe nanoparticles are produced on the substrate surface during these processes. Then deposition of BNNTs is initiated by focusing the laser beam on a high purity h-BN target propagating the BN vapor toward the substrates located near the target surface.

Scanning electron microscopy (SEM) shows that the BNNTs grown tend to form vertical bundles (Figure 6a). Figure 6b indicates the bundling configurations of BNNTs.

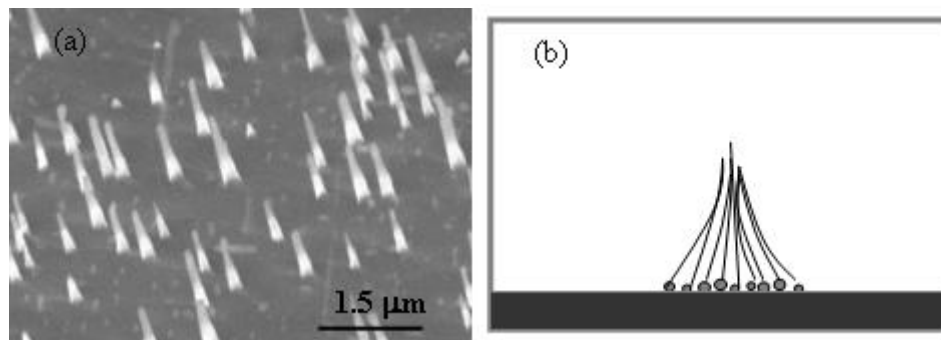


Figure 6. BNNTs grown directly on a substrate. (a) SEM image of BNNT bundles. (b) Cartoon depicting bundled nature of the tubes.

Transmission electron microscopy (TEM) was used to indicate the microstructure of BNNTs. Long and straight tubular structures were detected (Figure 7a). Figure 7b shows these BNNTs are made of high-order hexagonal phase h-BN shells with intershell spacing of 0.33nm.

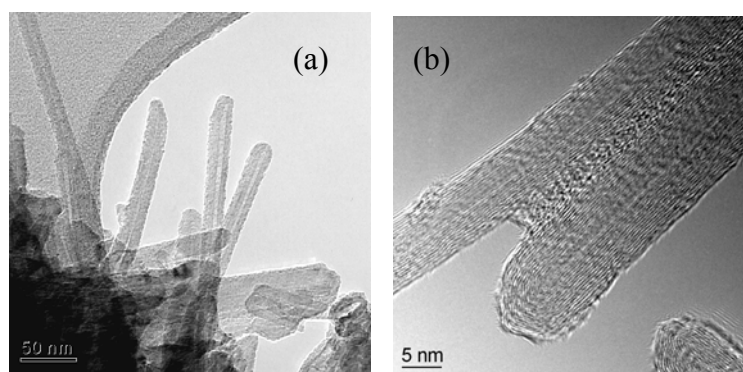


Figure 7. TEM images of the PE-PLD grown BNNTs. (a) The grown tubes are long and straight. (b) Higher magnifications reveal these tubes are highly ordered hexagonal BN shells. These two BNNTs are still in a bundle.

In summary, the synthesis of BNNTs on substrates has been achieved at the low temperature of 600 °C. Results shown here will stimulate future investigation of BNNTs and biological applications of BNNTs will start to gain momentum.

Zinc Oxide Nanotubes

Nanotubes of oxide and nitride materials are particularly interesting for their hydrophilic natures, their tubular structures and wide energy band gaps. They have enabled some exciting applications including photochemical cells (37), nanofluidic transistors (38), and DNA sensors (39) all of which have been demonstrated with the use of these nanotubes. The DNA sensors using silica nanotubes are based on the field effect transistor configuration and could in theory prove sensitive enough to detect and manipulate single biomolecules, something not available from CNTs.

For example, GaN (40), Silica (41), ZnO (42, 43), and TiO₂ (37) nanotubes have been synthesized by using multi-step processes with templates or hydrothermal techniques. Among these materials, ZnO nanotubes have generated significant interest due to their multifunctional properties for optical, electronic, and piezoelectric applications. ZnO nanotubes are expected to encompass the uses of other ZnO nanostructures for applications at the cutting edge of nanoscaling.

Crystal quality of materials is always important for their optimum physical properties and performance. Thus it is desired to establish techniques for the growth of single crystalline ZnO nanotubes. Based on the theory of nucleation and vapor-solid crystal growth, we have experimentally proven the direct growth of single crystalline ZnO nanotubes without the use of multiple processes, catalysts, or templates. According to the theory of nucleation, the probability of nuclei formation is highest at locations with maximum number of nearest neighbors. For flat 2D growth surfaces, higher binding energies for growth species occurred at the edges (44). For ZnO, it is well known that the growth rate along the *c*-axis is relatively faster (45, 46). At decreased growth temperatures, the nucleation probability and the surface migration will be suppressed (44). Thus if the growth temperatures are low enough to suppress migration along the 2D surface of the *c*-plane but high enough to sustain the growth along the *c*-axis, the condensation and growth will be limited at the edges of the *c*-plane of ZnO and form ZnO nanotubes.

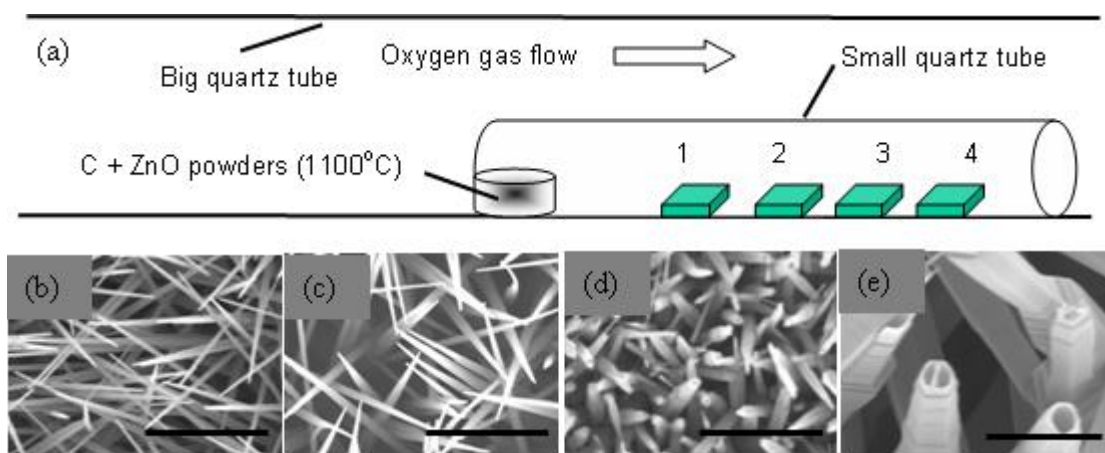


Figure 8. (a) Experimental setup in a double-tube horizontal furnace. No ZnO nanostructures were grown on substrate 1. Appearances of ZnO nanorods on substrates (b) 2, (c) 3, and ZnO nanotubes on (d) substrate 4. Scale bars are 6 microns. (e) Magnified view of ZnO nanotubes at a scale bar of 1 micron.

Based on this model, we have conducted a series of experiments to first start the growth of the *c*-surfaces of ZnO nanorods and then decrease the growth temperatures for the formation of the ZnO nanotubes by using a simple thermal CVD technique in a horizontal quartz tube vacuum chamber furnace. A smaller quartz tube containing the precursor materials and substrates was placed within the vacuum chamber. A mixture of ZnO and graphite powder in an alumina boat were the precursor materials and were placed at the closed end of the smaller quartz tube as shown in Figure 8 (a). A series of oxidized silicon substrates (numbered 1 to 4) were then placed down stream from the mixture in the small quartz tube before inserting it into the vacuum chamber such that the closed end was at the center of the furnace. The temperature of the furnace was raised to 1100°C, introducing oxygen at ~350°C. The temperature was held at 1100°C for 30 minutes and turned off to allow cooling to 600-700 °C in ~30 mins. Experiments were terminated by cooling the system to room temperature by opening the heating panel of the furnace. According to a calibration experiment, when the furnace is heated at 1100°C, the temperatures of substrates 1 to 4 are about 700°C, 600°C, 500°C, and 420°C, respectively. After the growth, all samples were examined by SEM.

In all these experiments, no coating was formed on substrate 1. ZnO Nanorods with sharp tips were grown on substrates 2 and 3 as shown in Figure 8 (b) and (c) respectively. We detected ZnO nanotubes only on substrates 4 as shown in Figure 8 (d). The diameters of these nanotubes are between ~100 to 500 nm near the opened tips as shown in Figure 8 (e). Some of these nanotubes have a single tubular channel as predicted by theory, though some have multiple channels. However, the formation of these multi-channel nanotubes is expected by the nucleation model discussed earlier. During the nucleation and growth, steps or vacancies could be formed at locations beyond the edges. Especially at suppressed growth temperatures, the formation of steps and vacancies will induce the formation of addition islands at these locations. These islands will tend to merge with the edges so as to reduce their surface energy (larger island, lower surface energy) (38). These processes are accompanied with the growth along the *c*-axis and thus transform the single channel nanotubes to multi-channel structures.

Figure 9 (a) shows the typical x-ray diffraction spectra of these nanotubes samples. These spectrum can be indexed for diffraction from the (002), (101), (102), and (103) planes of wurtzite crystals with lattice constants $a = 0.325\text{nm}$, and $c = 0.521\text{nm}$, which correspond to ZnO. The dominant (002) peak indicates that these ZnO nanotubes are preferentially grown in the [0001] direction since these nanotubes are partially vertically aligned on the substrates. The (101), (102) and (103) peaks may be induced by the imperfect vertical alignment as well as other trace nanostructures. We have further verified that these ZnO nanotubes are grown along the [0001] axis by TEM. Figure 9 (b) shows the hollow tubular tip of a ZnO nanotube at low resolution TEM. High resolution TEM images (not shown) indicate that these ZnO nanotubes are single crystals with the growth direction (arrows) aligned to the *c*-axis of ZnO with lattice spacing of 0.526 nm.

In short, we have demonstrated a promising route to growing single crystalline ZnO nanotubes, without catalysts and templates, by a conventional thermal CVD technique. These ZnO nanotubes were grown on the *c*-surfaces of ZnO nanorods as predicted by the theory of nucleation and vapor-solid crystals growth. In principle, the height of these nanorod bases can be minimized so that nanotubes with longer tubular section can be formed.

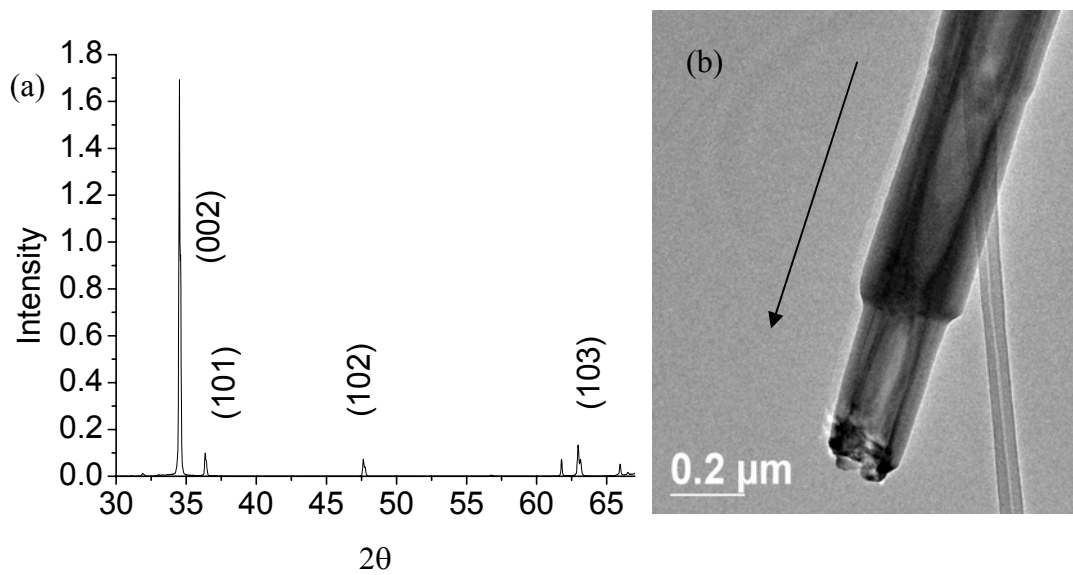


Figure 9. (a) XRD, and (b) TEM of a ZnO nanotubes. Arrow representing the c-axis of the nanotube.

Summary

It was shown that the progress in growing nanostructures affects our ability to use them for applications. In CNTs, growth is easy and controllable, leading to a wealth of study on biological applications. BNNTs, being similar to CNTs but more robust, are a promising material. Until recently, the difficulty of their growth has limited their use, but we have found easier, low-temperature growth methods that should help expand the scope of their application. Finally, ZnO materials are desired for their hydrophilic natures, their tubular structures and wide energy band gaps. These nanotubes can now be grown single-crystal by conventional thermal CVD methods, and, as continuing refinements of the growth techniques take place, they will find more and more use in biological applications.

Acknowledgments

This work is supported by Michigan Tech Research Excellent Funds, the US Department of Army (Grant No. W911NF-04-1-0029 through the City College of New York), National Science Foundation CAREER Award (Award number 0447555, Division of Materials Research), the U.S. Army Research Laboratory and the Defense Advanced Research Projects Agency (Contract number DAAD17-03-C-0115), and the Center for Nanophase Materials Science (CNMS) sponsored by the Division of Materials Sciences and Engineering, U.S. Department of Energy, under Contract No. DE-AC05-00OR22725 with UT-Battelle, LLC.

References

1. S. Iijima, *Nature* **354**, 56 (1991).
2. S.S. Wong, E. Joselevich, A.T. Woolley, C.L. Cheung and C.M. Lieber, *Nature*, **394**, 52 (1998).
3. N.W.S. Kam, Z. Liu and H. Dai, *Angew. Chem. Int. Ed.*, **44**, 1 (2005).
4. R.J. Chen, Y. Zhang, D. Wang and H. Dai, *J. Am. Chem. Soc.*, **123**, 3838 (2001).
5. C.V. Nguyen, L. Delzeit, A.M. Cassell, J. Li, J. Han and M. Meyyappan, *Nano Lett.*, **2**, 1079 (2002).
6. K. Besteman, J. Lee, G.M. Wiertz, H.A. Heering and C. Dekker, *Nano Lett.*, **3**, 727 (2003).
7. N.W.S. Kam, M. O'Connell, J.A. Wisdom and H. Dai, *PNAS*, **102**, 11600 (2005).
8. K. Wang, H.A. Fishman, H. Dai and J.S. Harris, *Nano Lett.*, **6**, 2043 (2006).
9. R. Singh, D. Pantarotto, L. Lacerda, G. Pastorin, C. Klumpp, M. Prato, A. Bianco and K. Kostarelos, *PNAS*, **103**, 3357 (2006).
10. G. W. Wagner and W. C. Ellis, *Appl. Phys. Lett.*, **4**, 89 (1964).
11. V. Kayastha, Y.K. Yap, S. Dimovski and Y. Gogotsi, *Appl. Phys. Lett.*, **85**, 15 (2004).
12. G.D. Lee, S. Han, J. Yu, and J. Ihm, *Phys. Rev. B*, **66**, 081403(R) (2002).
13. V.K. Kayastha, Y.K. Yap, Z. Pan, I.N. Ivanov, A.A. Puzosky and D.B. Geohegan; *Appl. Phys. Lett.*, **86**, 253105 (2005).
14. T. Hirao, K. Ito, H. Furuta, Y.K. Yap, T. Ikuno, S. Honda, Y. Mori, T. Sasaki and K. Oura, *Jpn. J. Appl. Phys.*, **40**, L631 (2001).
15. J. Menda, B. Ulmen, L.K. Vanga, V.K. Kayastha, Y.K. Yap, Z.Pan, I.N. Ivanov, A.A. Puzosky and D.B. Geohegan, *Appl. Phys. Lett.*, **87**, 173106 (2005).
16. N.G. Chopra et al., *Science*, **269**, 966 (1995).
17. A. Rubio, J.L. Corkill and M.L. Cohen, *Phys. Rev. B*, **49**, 5081 (1994).
18. K.H. Khoo, M.S.C. Mazzoni and S.G. Louie, *Phys. Rev. B*, **69**, 201401(R) (2004).
19. C.W. Chen, M.H. Lee and S.J. Clark, *Nanotechnology*, **15**, 1837 (2004).
20. M. Ishigami, J.D. Sau, S. Aloni, M.L. Cohen, and A. Zettl, *Phys. Rev. Lett.*, **94**, 56804 (2005).
21. Y. Chen, J. Zou, S.J. Campbell and G.L. Caer, *Appl. Phys. Lett.*, **84**, 2430 (2004).
22. E.J. Mele and P. Kra'1, *Phys. Rev. Lett.*, **88**, 56803 (2002).
23. S.M. Nakhmanson, A. Calzolari, V. Meunier, J. Bernholc and M.B. Nardelli, *Phys. Rev.*, **67**, 235406 (2003) .
24. S.H. Jhi and Y.K. Kwon, *Phys. Rev. B*, **69**, 245407 (2004).
25. C. Zhi, Y. Bando, C. Tang, R. Xie, T. Sekiguchi and D. Goldberg, *J. Am. Chem. Soc.*, **127**, 15996 (2005).
26. C. Zhi, Y. Bando, C. Tang, S. Honda, K. Sato, H. Kuwahara and D. Goldberg, *Angew. Chem. Int. Ed.*, **44**, 7923 (2005).
27. C. Zhi, Y. Bando, C. Tang and D. Goldberg, *J. Am. Chem. Soc.*, **127**, 17144 (2005).
28. C. Zhi, Y. Bando, C. Tang and D. Goldberg, *Phys. Rev. B*, **74**, 153413 (2006).
29. M. Terrones et al., *Chem. Phys. Lett.*, **259**, 568 (1996).
30. A. Loiseau, F. Willaime, N. Demoncy, G. Hug, and H. Pascard, *Phys. Rev. Lett.*, **76**, 4737 (1996).
31. D.P. Yu et al., *Appl. Phys. Lett.*, **72**, 1966 (1998).
32. R.S. Lee et al., *Phys Rev B*, **64**, 121405 (R) (2001).
33. W. Han, Y. Bando, K. Kurashima and T. Sato, *Appl. Phys. Lett.*, **73**, 3085 (1998).

34. Y. Chen, L.T. Chadderton, J.F. Gerald, and J.S. Williams, *Appl. Phys. Lett.*, **74**, 2960 (1999).
35. O.R. Lourie et al., *Chem. Mater.*, **12**, 1808 (2000).
36. J. Wang et al., *Nano Letters*, **5**, 2528 (2005).
37. G. K. Mor, K. Shankar, M. Paulose, O. K. Varghese and C. A. Grimes, *Nano Lett.*, **5**, 191 (2005).
38. R. Karnik, R. Fan, M. Yue, D. Li, P. Yang and A. Majumdar, *Nano. Lett.*, **5**, 943 (2005).
39. R. Fan, R. Karnik, M. Yue, D. Li, A. Majumdar, P. Yang, *Nano, Lett.* **5**, 1633 (2005).
40. J. Goldberger, R. He, Y. Zhang, S. Lee, H. Yan, H. J. Choi, and P. Yang, *Nature*, **422**, 599 (2003).
41. R. Fan, Y. Wu, D. Li, M. Yue, A. Majumdar, and P. Yang, *J. Am. Chem. Soc.*, **125**, 5254 (2003).
42. Y. Sun, G. M. Fuge, N. A. Fox, D. J. Riley, and M. N. R. Ashfold, *Adv. Mater.*, **17**, 2477 (2005).
43. G. S. Wu, T. Xie, X. Y. Yuan, Y. Li, L. Yang, Y. H. Xiao, L. D. Zhang, *Solid State Comm.*, **134**, 485 (2005).
44. I. Tarjan and M. Matrai, eds., "Laboratory Manual on Crystal Growth," Akadémiai Kiadó (Budapest, 1972) pp 29-30.
45. Y. Li, G. W. Meng, L. D. Zhang and F. Phillipp, *Appl. Phys. Lett.*, **76**, 2011 (2000).
46. M. H. Huang, Y. Wu, H. Feick, N, Tran, E. Weber and P. Yang, *Adv. Mater.*, **13**, 113 (2001).